Supporting Information for "Influence of fault zone maturity on fully dynamic earthquake cycles"

Prithvi Thakur[1] and Yihe Huang[1]

[1]University of Michigan, Department of Earth and Environmental Sciences

Table of Contents

Model Details and Parameter Space

Our damage evolution model is described by a change in the rigidity ratio with respect to the host rock. We parameterize this ratio of shear modulus of the damage zone to the shear modulus of the surrounding host rock using three variables: A: the coseismic damage accumulation, which shows the amount of damage increase after an earthquake, T: the healing time, which shows the interseismic duration it takes the fault zone to heal to its maximum level, and P: the permanent damage, which shows the amount of damage that the fault zone never recovers. The rigidity ratio evolves through time based on the following relation:

$$\frac{\mu_D}{\mu} = \begin{cases} A_0 - nP, & \text{after each earthquake} \\ A(1 - \exp(-T(t - t_{\text{start}}))) + A_0 - nP, & \text{during interseismic period} \end{cases} \tag{1}$$

where t and t_{start} are the current timestep and the start time of the previous earthquake in years, $\frac{1}{T}$ is the inverse of healing time (in years), A_0 is the prescribed damage after the earthquake. For the simulations with zero permanent damage (Figure 2 and Figure 3), A_0 is constant and prescribed based on the level of fault maturity, while P is set to 0. For the simulation with permanent damage (Figure S1), the permanent damage P is set up by decreasing A_0 after each earthquake to $A_0 - nP$, where n is the earthquake number, and the initial P is set such that the net rigidity drop after an earthquake is 1 %.

We use a spectral element method to simulate fully dynamic ruptures and aseismic deformation on a two-dimensional fault with mode-III rupture (Kaneko et al., 2011; Thakur et al., 2020). Adaptive time-stepping is used to switch from aseismic to seismic events based on a threshold slip velocity of $0.5\,\text{mm}\,\text{s}^{-1}$ (Erickson et al., 2020). The fault is 24 km deep, with the seismogenic zone extending from 3 km to 16 km. The rest of the fault creeps aseismically. Our two-dimensional rectangular domain is twice the fault-length in the dip direction and 30 km in the off-fault direction. The bottom of the fault is loaded with a plate loading rate of $35\,\mathrm{mm\,yr^{-1}}$. Free surface is imposed on the top boundary of the domain, whereas the other three boundaries have absorbing boundary conditions. The frictional resistance of the fault to sliding is described by laboratory derived rate- and state-dependent friction laws, which were developed empirically (Dieterich, 1979; Ruina, 1983; Blanpied et al., 1991) and is widely used in numerical models to simulate earthquake sequences (Rice, 1993; Lapusta et al., 2000). We use rate- and state- dependent friction with aging law for the state-evolution to simulate earthquake sequences on the fault (Dieterich, 1979; Ruina, 1983; Scholz, 1998). We use the regularized form of the rate-and-state model (Lapusta et al., 2000; Rice & Ben-Zion, 1996), which relates the shear strength (T) to the slip rate ($\dot{\delta}$) as follows:

$$T = a\bar{\sigma}\,\mathrm{arcsinh}\left[\frac{\dot{\delta}}{2\dot{\delta}_o} e^{\frac{f_o + b\ln(\dot{\delta}\theta/L)}{a}}\right] \tag{2}$$

where $\bar{\sigma}$ is the effective normal stress (i.e., the difference between lithostatic stress and the pore fluid pressure), f_o is a reference friction coefficient corresponding to a reference slip rate $\dot{\delta}_o$, L is the characteristic distance over which the contact asperity slips, and a and b are empirical constants dependent on the mechanical and thermal properties of the contact surface. The state variable θ, interpreted as the average lifetime of the contact asperity, evolves as follows:

$$\frac{d\theta}{dt} = 1 - \frac{\dot{\delta}\theta}{L} \tag{3}$$

(Barbot, 2019) has shown that the state variable θ is the age of contact strengthening. Depending on the values of L, $(a-b)$, and the ratio $\frac{a}{b}$, we can determine the frictional stability of the fault wherein we can have an unstable slip for a steady state velocity weakening frictional regime ($a - b < 0$), or a stable sliding for a steady state velocity strengthening frictional regime ($a - b > 0$). Fault dynamics is controlled by R_u, the ratio of the velocity-weakening patch size to the nucleation size, and the ratio $\frac{b-a}{a}$ that controls the relative importance of strengthening and weakening effects and the ratio of static to dynamic stress drops. For higher values of R_u, we can obtain more chaotic rupture styles such as partial and full ruptures, aftershock sequence, and a wide range of events (Barbot, 2019; Cattania, 2019). In our simulations, we use relatively simple values for the theoretical nucleation size of $\sim$ 2 km, and the width of velocity weakening region of $\sim$ 10 km, implying that the value of R_u is ~ 5, which predicts single-period full ruptures in a homogeneous medium (Barbot, 2019). Previous studies (Lapusta & Rice, 2003; Cattania, 2019) have shown that earthquake complexities and partial ruptures increases as the nucleation size becomes smaller compared to the fault length. These studies consider quasidynamic simulations in a homogeneous medium. (Thakur et al., 2020) have further shown that a layered elastic compliant zone in earthquake cycle simulations with full inertial effects show additional complexities due to dynamic wave reflections and stress heterogeneities, which are absent in an equivalent homogeneous simulation with comparable R_u number. In this study, our choice of the characteristic fault length ($L = 8\,\mathrm{mm}$), and the choice of rigidity ratios (which is inspired from seismic studies of real fault zone observations) ensures that even for the largest Dieterich-Ruina-Rice number (i.e., the most compliant and most mature fault zones), an equivalent homogeneous medium would give characteristic events. We design these models to isolate the effects of coseismic damage accumulation and interseismic healing in fault zones of different maturity, while keeping the frictional complexities at a minimum.

The fault damage zone extends throughout the domain and is symmetric across the fault. We use temporal changes in the rigidity ratio of the fault damage zone for modeling the damage accumulation and healing through time. We use a constant half-width of 1 km for the fault zone geometry. This facilitates easier comparison between mature and immature fault zones and is coherent with the observations (Ben-Zion & Sammis, 2003; Perrin et al., 2016). The host rock has a shear wave velocity of 3464 km/s and a density of 2670 $\mathrm{kgm^{-3}}$ implying that the shear modulus is 32 GPa. We start with the same initial shear wave velocity in the fault damage zone but with a density of 2500 $\mathrm{kgm^{-3}}$ which remains constant throughout the simulation (Kaneko et al., 2008; Kaneko et al., 2011). Since density does not contribute as much to the rigidity as the shear wave velocity, any changes in the rigidity of the fault damage zone are directly related to the changes in shear wave velocity, which is an observable from seismic monitoring experiments. The initial rigidity ratio ($\frac{\mu_D}{\mu}$) is approximately 0.94, which primarily stems from the density difference between the host rock and the fault damage zone. The parameters tested for this study are discussed in Tables S1 and S2. The parameters shown in the results are shown in bold in Table S2.

The time-evolution of the shear modulus, described in equation A1, is operative only during the quasi-static part of the deformation, i.e., when the inertia is negligible and the fault is creeping aseismically. Since the time-steps are large in this part of the simulation, the deformation is essentially slow-enough such that the stress-strain relationship is linear throughout the numerical simulation. During the dynamic earthquakes, the shear modulus remains constant till the inertial effects are dissipated, after which it drops by a prescribed amount. This ensures that we can study the effects of coseismic damage accumulation and interseismic healing using parameters inspired by seismic observations, but still pertain to an elastic deformation regime. The effects of damage generation and healing in our simulations is modeled purely as an elastic effect. We ignore the dissipative effects of coseismic damage generation as well as plastic strain in off-fault. The variation in fault-slip behavior in our models result primarily from compliance contrast in an elastic framework, but also from how the aseismic slip builds up as the fault zone heals. The nucleation process is similar for both mature and immature fault zones in our models, with the differences only arising from compliance contrast, but how the rupture terminates and therefore the location of residual stress peaks are significantly different in our models with mature and immature fault zones. Furthermore, the rupture propagation style is very different for these models as discussed in Section 3.1. This difference in rupture propagation style purely due to compliance contrast has been studied previously for single earthquake ruptures (Huang & Ampuero, 2011; Huang et al., 2014). The effects of slip accumulation during the coseismic phase is predominant in mature fault zone models whereas the effects of slip accumulation during the interseismic creep phase is predominant in immature fault zone models. Both of these influence the stress peaks and therefore where the rupture nucleates and terminates.

Figure S1 shows the fault-slip evolution in a simulation that includes permanent damage after each earthquake.

Table S1. Parameters used in numerical simulations of earthquake cycles. The normal and shear stresses represent the values for the velocity-weakening region.

Parameter	Symbol	Value
Static friction coefficient	μ_0	0.6
Reference velocity	V_0	$1 \times 10^{-6}\,\mathrm{m\,s^{-1}}$
Plate loading rate	V_{pl}	$35\,\mathrm{mm\,yr^{-1}}$
Evolution effect	b	0.019
Effective normal stress	$\bar{\sigma}$	50 MPa
Initial shear stress	τ_0	30 MPa
Steady-state velocity dependence		
in the seismogenic region	$(b-a)$	-0.004
Width of seismogenic zone	W	10 km
Half-width of damage zone	W	0.5 km
Average node spacing	dx	20 m
Seismic slip-rate threshold	V_{th}	$1\,\mathrm{mm\,s^{-1}}$
Characteristic weakening distance	L_c	8 mm
Shear modulus of host rock	μ	32 GPa
Shear modulus of damaged rock	μ_D	Variable (see Eq. A1)

Table S2. Damage evolution and healing parameters. The parameters in bold represent the simulations presented in the paper. The left column shows the range of rigidity ratio over which the shear modulus drops during earthquake and heals during interseismic period.

Rigidity ratio ($\frac{\mu_D}{\mu}$)	Healing time (yr)
40 – 45%	**8**, 10, 12, 15
80 – 85%	**8**, 10, 12, 15
60 – 65%	4, **8**, 10, 20
60 – 70%	8
60 – 80%	8

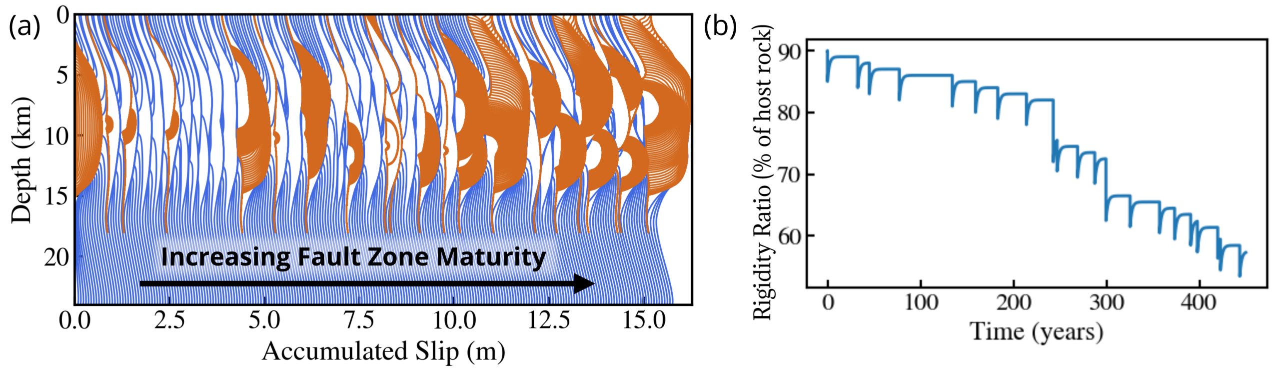

Figure S1. Incorporation of permanent damage after each earthquake demonstrates the transition from immature to mature fault zone. (a) The accumulated slip history. (b) Rigidity ratio through time. Here, the transition from immature to mature fault zone occurs within a few hundred years, whereas in nature, the evolution can take millions of years.

References

Barbot, S. (2019). Slow-slip, slow earthquakes, period-two cycles, full and partial ruptures, and deterministic chaos in a single asperity fault. *Tectonophysics*, *768*, 228171.

Ben-Zion, Y., & Sammis, C. G. (2003). Characterization of fault zones. *Pure and Applied Geophysics*, *160*(3-4), 677–715.

Blanpied, M., Lockner, D., & Byerlee, J. (1991). Fault stability inferred from granite sliding experiments at hydrothermal conditions. *Geophysical Research Letters*, *18*(4), 609–612.

Cattania, C. (2019). Complex earthquake sequences on simple faults. *Geophysical Research Letters*, *46*(17-18), 10384–10393.

Dieterich, J. H. (1979). Modeling of rock friction: 1. experimental results and constitutive equations. *Journal of Geophysical Research: Solid Earth*, *84*(B5), 2161-2168. Retrieved from https://agupubs.onlinelibrary.wiley.com/doi/abs/10.1029/JB084iB05p02161 doi: 10.1029/JB084iB05p02161

Erickson, B. A., Jiang, J., Barall, M., Lapusta, N., Dunham, E. M., Harris, R., ... others (2020). The community code verification exercise for simulating sequences of earthquakes and aseismic slip (seas). *Seismological Research Letters*, *91*(2A), 874–890.

Huang, Y., & Ampuero, J.-P. (2011). Pulse-like ruptures induced by low-velocity fault zones. *Journal of Geophysical Research: Solid Earth*, *116*(B12). Retrieved 2021-04-30, from `https://agupubs.onlinelibrary.wiley.com/doi/abs/10.1029/2011JB008684` (_eprint: https://agupubs.onlinelibrary.wiley.com/doi/pdf/10.1029/2011JB008684) doi: https://doi.org/10.1029/2011JB008684

Huang, Y., Ampuero, J.-P., & Helmberger, D. V. (2014). Earthquake ruptures modulated by waves in damaged fault zones. *Journal of Geophysical Research: Solid Earth*, *119*(4), 3133–3154.

Kaneko, Y., Ampuero, J.-P., & Lapusta, N. (2011, October). Spectral-element simulations of long-term fault slip: Effect of low-rigidity layers on earthquake-cycle dynamics. *Journal of Geophysical Research (Solid Earth)*, *116*, B10313. doi: 10.1029/2011JB008395

Kaneko, Y., Lapusta, N., & Ampuero, J.-P. (2008). Spectral element modeling of spontaneous earthquake rupture on rate and state faults: Effect of velocity-strengthening friction at shallow depths. *Journal of Geophysical Research: Solid Earth*, *113*(B9).

Lapusta, N., & Rice, J. R. (2003). Nucleation and early seismic propagation of small and large events in a crustal earthquake model. *Journal of Geophysical Research: Solid Earth*, *108*(B4).

Lapusta, N., Rice, J. R., Ben-Zion, Y., & Zheng, G. (2000). Elastodynamic analysis for slow tectonic loading with spontaneous rupture episodes on faults with rate- and state-dependent friction. *Journal of Geophysical Research: Solid Earth*, *105*(B10), 23765-23789. Retrieved from https://agupubs.onlinelibrary.wiley.com/doi/abs/10.1029/2000JB900250 doi: 10.1029/2000JB900250

Perrin, C., Manighetti, I., Ampuero, J.-P., Cappa, F., & Gaudemer, Y. (2016). Location of largest earthquake slip and fast rupture controlled by along-strike change in fault structural maturity due to fault growth. *Journal of Geophysical Research: Solid Earth*, *121*(5), 3666-3685. Retrieved from https://agupubs.onlinelibrary.wiley.com/doi/abs/10.1002/2015JB012671 doi: 10.1002/2015JB012671

Rice, J. R. (1993). Spatio-temporal complexity of slip on a fault. *Journal of Geophysical Research: Solid Earth*, *98*(B6), 9885–9907.

Rice, J. R., & Ben-Zion, Y. (1996). Slip complexity in earthquake fault models. *Proceedings of the National Academy of Sciences*, *93*(9), 3811–3818.

Ruina, A. (1983). Slip instability and state variable friction laws. *Journal of Geophysical Research: Solid Earth*, *88*(B12), 10359-10370. Retrieved from https://agupubs.onlinelibrary.wiley.com/doi/abs/10.1029/JB088iB12p10359 doi: 10.1029/JB088iB12p10359

Scholz, C. H. (1998). Earthquakes and friction laws. *Nature*, *391*(6662), 37.

Thakur, P., Huang, Y., & Kaneko, Y. (2020, August). Effects of Low-Velocity Fault Damage Zones on Long-Term Earthquake Behaviors on Mature Strike-Slip Faults. *Journal of Geophysical Research: Solid Earth*, *125*(8). Retrieved 2021-04-30, from https://onlinelibrary.wiley.com/doi/10.1029/2020JB019587 doi: 10.1029/2020JB019587